Reassessment of the phylogenetic relationships of the late Miocene apes *Hispanopithecus* and *Rudapithecus* based on vestibular morphology

Alessandro Urciuoli[a,1], Clément Zanolli[b], Sergio Almécija[a,c,d], Amélie Beaudet[a,e,f,g], Jean Dumoncel[h], Naoki Morimoto[i], Masato Nakatsukasa[i], Salvador Moyà-Solà[a,j,k], David R. Begun[l], and David M. Alba[a,1]

[a]Institut Català de Paleontologia Miquel Crusafont, Universitat Autònoma de Barcelona, 08193 Barcelona, Spain; [b]Univ. Bordeaux, CNRS, MCC, PACEA, UMR 5199, F-33600 Pessac, France; [c]Division of Anthropology, American Museum of Natural History, New York, NY 10024; [d]New York Consortium in Evolutionary Primatology, New York, NY 10016; [e]Department of Archaeology, University of Cambridge, Cambridge CB2 1QH, United Kingdom; [f]School of Geography, Archaeology, and Environmental Studies, University of the Witwatersrand, Johannesburg, WITS 2050, South Africa; [g]Department of Anatomy, University of Pretoria, Pretoria 0001, South Africa; [h]Laboratoire Anthropology and Image Synthesis, UMR 5288 CNRS, Université de Toulouse, 31073 Toulouse, France; [i]Laboratory of Physical Anthropology, Graduate School of Science, Kyoto University, 606 8502 Kyoto, Japan; [j]Institució Catalana de Recerca i Estudis Avançats, 08010 Barcelona, Spain; [k]Unitat d'Antropologia, Departament de Biologia Animal, Biologia Vegetal i Ecologia, Universitat Autònoma de Barcelona, 08193 Barcelona, Spain; and [l]Department of Anthropology, University of Toronto, Toronto, ON M5S 2S2, Canada

Edited by Justin S. Sipla, University of Iowa, Iowa City, IA, and accepted by Editorial Board Member C. O. Lovejoy December 3, 2020 (received for review July 19, 2020)

Late Miocene great apes are key to reconstructing the ancestral morphotype from which earliest hominins evolved. Despite consensus that the late Miocene dryopith great apes *Hispanopithecus laietanus* (Spain) and *Rudapithecus hungaricus* (Hungary) are closely related (Hominidae), ongoing debate on their phylogenetic relationships with extant apes (stem hominids, hominines, or pongines) complicates our understanding of great ape and human evolution. To clarify this question, we rely on the morphology of the inner ear semicircular canals, which has been shown to be phylogenetically informative. Based on microcomputed tomography scans, we describe the vestibular morphology of *Hispanopithecus* and *Rudapithecus*, and compare them with extant hominoids using landmark-free deformation-based three-dimensional geometric morphometric analyses. We also provide critical evidence about the evolutionary patterns of the vestibular apparatus in living and fossil hominoids under different phylogenetic assumptions for dryopiths. Our results are consistent with the distinction of *Rudapithecus* and *Hispanopithecus* at the genus rank, and further support their allocation to the Hominidae based on their derived semicircular canal volumetric proportions. Compared with extant hominids, the vestibular morphology of *Hispanopithecus* and *Rudapithecus* most closely resembles that of African apes, and differs from the derived condition of orangutans. However, the vestibular morphologies reconstructed for the last common ancestors of dryopiths, crown hominines, and crown hominids are very similar, indicating that hominines are plesiomorphic in this regard. Therefore, our results do not conclusively favor a hominine or stem hominid status for the investigated dryopiths.

inner ear | semicircular canals | evolution | fossil apes | Hominidae

Hominoids (apes and humans) originated in Africa during the Oligocene (1) but subsequently dispersed into Eurasia, giving rise to an impressive radiation during the middle and late Miocene (2, 3). Thus, while extant hominoids include only two moderately diverse families—hylobatids (gibbons and siamangs) and hominids (great apes and humans)—the panoply of extinct genera recorded during the Miocene still defies classification into a coherent systematic scheme. Other than the late Miocene *Oreopithecus*—which might be a late-occurring stem hominoid (4, 5)—there is consensus that most Eurasian large-bodied hominoids are members of the great-ape-and-human clade (Hominidae) (2, 3, 6). While most Asian extinct great apes, such as *Sivapithecus*, are considered to be more closely related to the orangutan clade (Ponginae) than to African apes and humans (Homininae) (2, 6–8), the phylogenetic affinities of European *Dryopithecus* and allied forms have long been debated. Until a decade ago, several species of European apes from the middle and late Miocene were included within this genus (9–16). However, discoveries at the middle Miocene composite section of Abocador de Can Mata (6, 17–20) prompted the recognition that the late Miocene species belong to one or more different genera distinct from *Dryopithecus* (2, 3, 6, 7, 18, 21–26): *Hispanopithecus* from Spain and *Rudapithecus* from Hungary, the latter formerly considered a subgenus of the former by some authors (6, 18, 22).

Together with *Dryopithecus* and other middle to late Miocene taxa (17, 19, 27), *Hispanopithecus* and *Rudapithecus* are currently classified in a subfamily (Dryopithecinae) (6, 20, 26) or tribe (Dryopithecini) (3, 7, 21) of their own, distinct from pongines. Both taxa possess a hominid-like cranial morphology (6, 11–13, 21, 25, 28, 29), as shown by the high zygomatic root, reduced midfacial prognathism, lack of subarcuate fossa, deep glenoid

Significance

Reconstructing the phylogenetic relationships of extinct apes is challenging due to their fragmentary fossil record and the recurrent independent evolution of morphological features. Given the relevance of the phylogenetic signal of the bony labyrinth, here we assess the phylogenetic affinities of the late Miocene great apes *Hispanopithecus* and *Rudapithecus* by studying their inner ear morphology. Our results are consistent with the distinct generic status of these dryopiths, which further differ from the derived condition of orangutans and most closely resemble African apes. However, the latter appear largely primitive (similar to the last common ancestor of great apes and humans). Hence, our results do not conclusively favor a closer relationship with African apes as opposed to great apes as a whole.

Author contributions: A.U., S.M.-S., D.R.B., and D.M.A. designed research; A.U. and C.Z. performed research; A.U., C.Z., A.B., J.D., N.M., M.N., and D.R.B. contributed new reagents/analytic tools; A.U., C.Z., S.A., A.B., J.D., and D.M.A. analyzed data; and A.U., C.Z., and D.M.A. wrote the paper.

The authors declare no competing interest.

This article is a PNAS Direct Submission. J.S.S. is a guest editor invited by the Editorial Board.

[1]To whom correspondence may be addressed. Email: alessandro.urciuoli@icp.cat or david.alba@icp.cat.

This article contains supporting information online at https://www.pnas.org/lookup/suppl/doi:10.1073/pnas.2015215118/-/DCSupplemental.

Published January 25, 2021.

fossa, and prominent entoglenoid process. However, there is no consensus regarding the phylogenetic position of this group—being either considered stem hominids (6, 19, 30), stem hominines (2, 3, 14, 16, 25), or even pongines (10, 28, 29)—which may be informally referred to as "dryopiths." Resolving the phylogenetic position of dryopiths has important implications for the evolution of the great ape and human clade, since their purported hominine status has led to paleobiogeographic scenarios favoring a European origin and subsequent back-to-Africa dispersal for the African and human clade (2, 3, 15, 24, 25). Disagreements and uncertainties about the phylogenetic position of extinct apes are persistent, and stem from a combination of factors, including the incomplete and fragmentary hominoid fossil record, the decimated current diversity of the group, and pervasive homoplasy coupled with mosaic evolution (6, 23, 31–35).

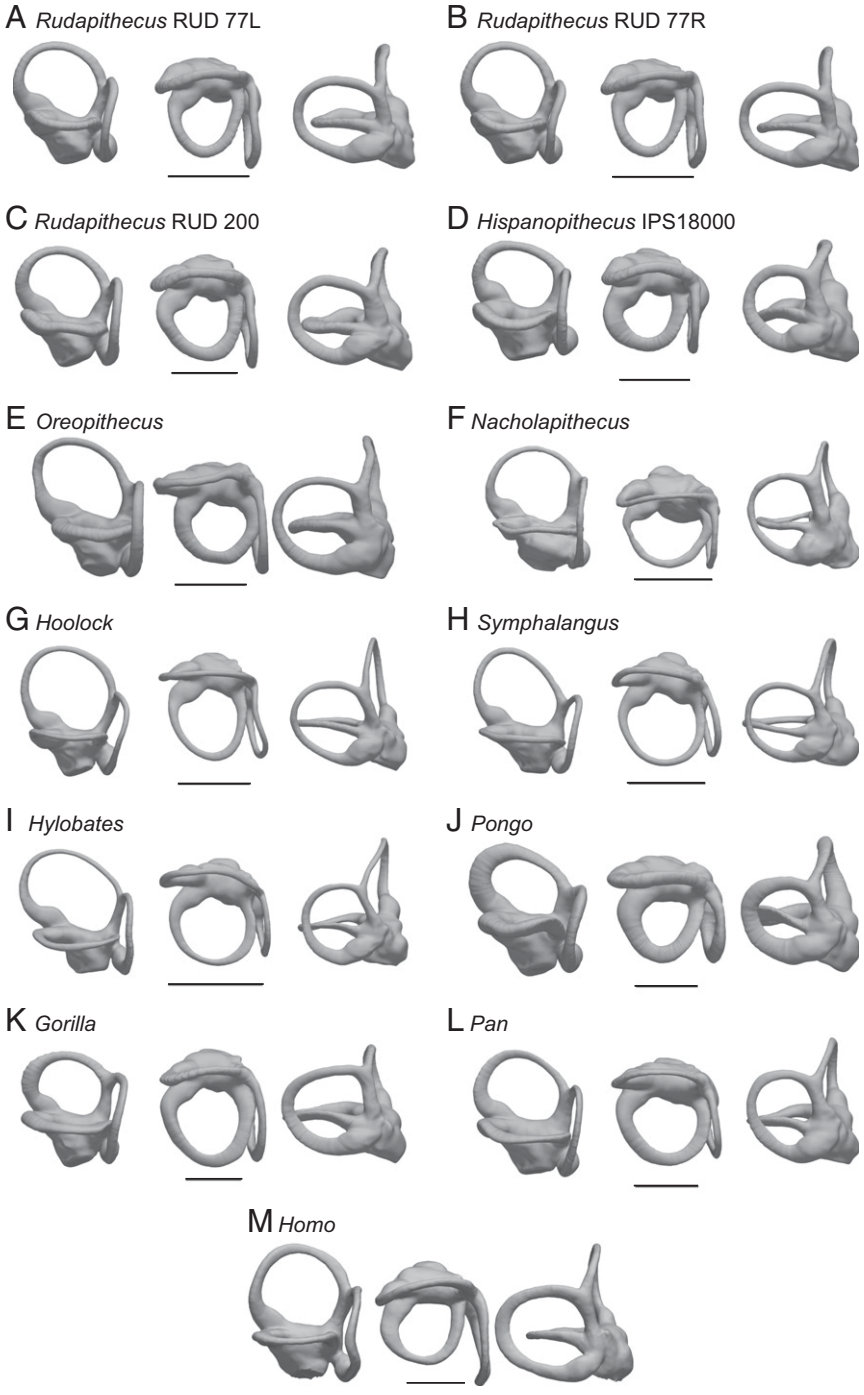

Fig. 1. The vestibular apparatus morphology of *R. hungaricus* (*A*–*C*), *H. laietanus* (*D*), fossil hominoids (*E* and *F*), and individuals from extant hominoid genera (*G*–*M*) as depicted by renderings of the 3D models. From left to right, in posterolateral, superior, and posteromedial views: (*A*) *R. hungaricus* (RUD 77L); (*B*) *R. hungaricus* (RUD 77R); (*C*) *R. hungaricus* (RUD 200); (*D*) *H. laietanus* (IPS18000); (*E*) *Oreopithecus bambolii* (BAC 208); (*F*) *N. kerioi* (BG 42744); (*G*) *Hoolock hoolock* (AMNH.M 83425); (*H*) *Symphalangus syndactylus* (AMNH.M 106583); (*I*) *Hylobates lar* (MCZ 41424); (*J*) *Pongo* sp.(IPS10647); (*K*) *Gorilla gorilla* (AMNH.M 167338); (*l*) *Pan troglodytes* (AMNH.M 51204); (*M*) *Homo sapiens* (F 04). (Scale bars, 5 mm.)

The morphology of the semicircular canals (SCs), which partly constitute the inner ear's bony labyrinth, has been classically related to locomotion (36–42). However, several studies have highlighted the possibility of inferring phylogenetic relatedness based on this portion of the inner ear morphology (43–47). Recently, it has been shown that this anatomical structure also embeds a strong phylogenetic signal among catarrhine primates by means of three-dimensional geometric morphometric (3DGM) analyses (5, 47–49), thus being potentially useful to test phylogenetic hypotheses for extinct hominoids. Previous studies relied on the SC radius of *Rudapithecus hungaricus* and *Hispanopithecus laietanus* to infer slow and deliberate arboreal locomotion for these species (41). However, recent analyses raised doubts about the reliability of locomotor behavior predictions based on the SC radius only (50, 51). In contrast, here we rely on microcomputed tomography (μCT) scans of the same specimens and a deformation-based (landmark-free) 3DGM approach to assess their closest affinities in SC morphology with extant hominoids and interpret them from an evolutionary viewpoint. First, we describe the fossil remains and qualitatively compare them with extant hominoids. Second, we assess if the volumetric proportions of their SCs more closely resemble those of hominids than those of other anthropoids. Third, we quantitatively evaluate changes in SC and vestibule morphology by means of a between-group principal component analysis (bgPCA) applied to a sample of extant and extinct hominoids. The affinities of the investigated fossil taxa are further assessed by means of cluster analyses and group membership probabilities based bgPCA results. Finally, we reconstruct the evolutionary history of the hominoid SCs using a phylomorphospace approach (including reconstructed ancestral morphotypes) under various phylogenetic assumptions for dryopiths.

Results

Descriptions and Comparisons. Three-dimensional renderings of the vestibular apparatus of fossil and extant hominoids investigated here are illustrated in the Fig. 1. The vestibular apparatus of *R. hungaricus* is well preserved in the three available specimens (Fig. 1 *A*–*C*). As in extant hominids, the SCs are stout—although less so than in orangutans (Fig. 1*J*), most humans (Fig. 1*M*), and gorillas (Fig. 1*K*)—and the vestibule is large relative to the volume occupied by SCs. The anterior and posterior canals are large and similar in size (Fig. 1 *A* and *B*). The anterior canal is slightly vertically compressed, as in extant hominoids and the fossil apes *Nyanzapithecus alesi* (4) and *Nacholapithecus kerioi* (Fig. 1*F*), and somewhat larger in RUD 77 than in RUD 200. The anterior canal is somewhat anterosuperiorly projecting, albeit much less so than in *Pongo* (Fig. 1*J*) and *Oreopithecus* (Fig. 1*E*). The lateral and posterior canals are slightly different between the two individuals. In RUD 77, the lateral canal is noticeably smaller than the other SCs (Fig. 1 *A* and *B*), slightly compressed horizontally, and slenderer than in RUD 200. The lateral canal of RUD 200 is stout and large, almost reaching the size of the vertical SCs (similar to the condition in African apes, yet smaller than in gorillas) (Fig. 1*C*), and its slender portion connects with the vestibule somewhat more inferiorly than in RUD 77. The junction of the slender portion of the lateral canal and the ampulla further differs between the two individuals, as it protrudes anteriorly in RUD 200, while it is posterolaterally oriented in RUD 77. In both individuals, the ampullary portion bends superiorly and the slender segment between the connection with the vestibule and the posterolateral tip of the lateral canal is straight, as in *Hoolock* (Fig. 1*G*) and in most hominids (Fig. 1 *J*–*M*), except for some *Gorilla* and *Pan* specimens that show some curvature. However, this section of the canal is more laterally oriented in RUD 77, while it is almost parallel to the posterior canal in RUD 200. The posterior canal is elongated posterolaterally in RUD 77, as in gorillas (Fig. 1*K*) and some humans (Fig. 1*M*), while it is slightly more rounded in RUD 200 (Fig. 1*C*). In both RUD 77 and RUD 200, the posterior and lateral canals approximately define a right angle (slightly more obtuse in RUD 77) and the trajectory of the lateral canal does not intersect the plane identified by the posterior canal. The common crus (CC) is short and slender, with the slender portions of the anterior and posterior canals almost forming right angle at the CC apex. The SCs are almost coplanar, with a slight amount of torsion in the upper portion of the anterior one (the tip slightly bending medially), in the medial-most part of the posterior one (displaced anteriorly), and in the tip of the lateral canal (pointing inferiorly).

The vestibular apparatus of *H. laietanus* (Fig. 1*D*) differs from that of *Rudapithecus* (especially RUD 77) (Fig. 1 *A* and *B*) by being more voluminous and displaying more equally developed SCs. The larger volume is particularly appreciable on the vestibular recesses (which are more voluminous than the SCs, as in orangutans) (Fig. 1*J*) and in the much more inflated ampullae. The anterior canal is more vertically compressed than in *Rudapithecus*, showing an almost rectangular shape. This canal is also much slenderer than in orangutans (Fig. 1*J*) and gorillas (Fig. 1*K*), most closely resembling chimpanzees (Fig. 1*L*). The lateral canal is stouter than the others, especially in the ampullary portion. Its posterolateral-most tip slightly bends inferiorly, resulting in a moderate torsion of the canal. The slender segment between the connection with the vestibule and the posterolateral tip of the lateral canal is straight, as in *Rudapithecus* (Fig. 1 *A*–*C*), *Hoolock* (Fig. 1*G*), and most hominids (Fig. 1 *J*–*M*), and laterally oriented, as in *Pongo* (Fig. 1*J*), some humans (Fig. 1*M*), and RUD 77 (Fig. 1 *A* and *B*). The ampullary portion of the lateral canal is bent superiorly, as in *Rudapithecus* (Fig. 1 *A*–*C*) and extant hominoids (Fig. 1 *G*–*M*). However, unlike extant great apes (Fig. 1 *J*–*L*) and *Rudapithecus* (Fig. 1 *A*–*C*), the portion between the ampulla and the tip of the lateral canal is inflated. The posterior canal is small and rounded, with a large ampulla. The CC is longer than in *Rudapithecus* (Fig. 1 *A*–*C*) and in most extant great apes (with *Pongo* showing the shortest), yet more inflated (even if much less so that in orangutans) (Fig. 1*J*), and the CC apex forms an obtuse angle. As in *Rudapithecus* and extant hominids, the planes identified by the lateral and posterior canals form a right angle and their trajectories do not intersect.

Volumetric Proportions. Allometric regressions of SC volume vs. length were performed separately for hominoids and the rest of anthropoids included in the sample (Fig. 2*A*; measurements for the dryopiths are given in *SI Appendix*, Table S1), because it has been previously shown that the former display an allometric grade shift toward relatively higher volumes at a comparable length once size-scaling effects have been taken into account (5), with only minimal overlap. *Hispanopithecus* falls above the hominid regression line, while *Rudapithecus* is situated more (RUD 77) or less (RUD 200) below the line, close to *Nacholapithecus*, but in all cases within the range of extant hominids and well above the regression line of other anthropoids (Fig. 2*A*). Gorillas are variable in this regard, while humans and orangutans display stouter proportions than chimpanzees and bonobos (Fig. 2*B*). The SCs of *Hispanopithecus* appear intermediate between these aforementioned taxa (closer to humans and orangutans), while those of *Rudapithecus*, *Oreopithecus*, and *Nacholapithecus* are slenderer and more comparable to those of chimpanzees and bonobos. Overall, given their range of variation, all the extinct apes analyzed here display extant hominid-like volumetric proportions of the vestibular apparatus.

Shape Analysis. The bgPCA (Fig. 3), based on the deformation fields computed for the hominoid sample, allows us to discriminate extant hominoid species, as shown by classification results

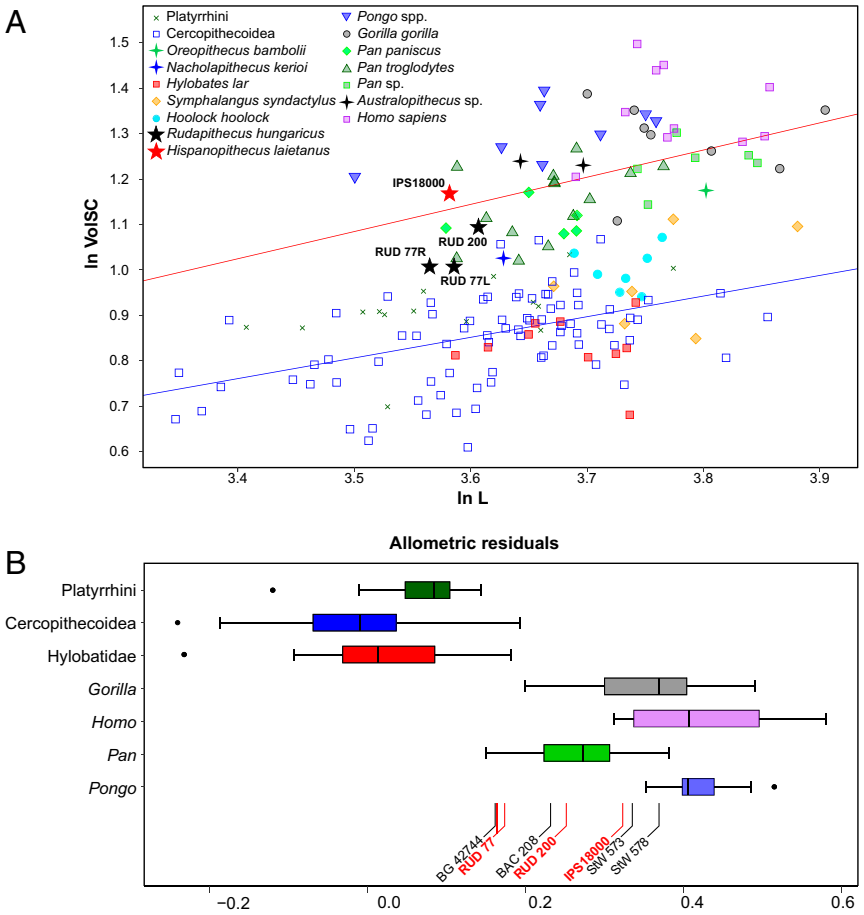

Fig. 2. (*A*) Allometric regressions of cube root of SC volume (ln VolSC, in millimeters) vs. SC length (ln L, in millimeters) in anthropoids. Lines represent ordinary least-squares best-fit lines for extant hominids (red) and other extant anthropoids (blue). Both hominids and other anthropoids show a negatively allometric relationship between VolSC and L, but with a marked allometric grade shift, such that hominids possess stouter canals than other anthropoid taxa at comparable lengths (see *SI Appendix*, Table S1 for comparative sample measurements). (*B*) Boxplots of allometric residuals computed using the best-fit line of the nonhominid anthropoid regression as baseline. Horizontal line is the median, boxes represent the interquartile range, whiskers represent maximum and minimum excluding outliers (beyond 1.5 times the upper and lower quartiles), and black dots are outliers. Samples for each boxplot are: Platyrrhini (n = 15), Cercopithecoidea (n = 80), Hylobatidae (n = 23), *Gorilla* (n = 8), *Pongo* (n = 8), *Pan* (n = 25), and *Homo* (n = 10). Note that all the fossils overlap with extant hominoids. However, while *Australopithecus* (StW 573 and StW 578) and *Hispanopithecus* (IPS18000) approach the human and orangutan condition, *Rudapithecus* RUD 200 and *Oreopithecus* (BAC 208) only overlap with African apes, while *Nacholapithecus* (BG 42744) and *Rudapithecus* RUD 77 only overlap with chimpanzees and bonobos, and marginally also with the upper range of hylobatids and cercopithecoids.

(99% of correctly classified individuals before and after cross-validation). These results closely resemble those computed using a cross-validated bgPCA (*SI Appendix*, Fig. S1). We also recover very significant group mean differences ($P < 0.001$) for the raw shape data (*SI Appendix*, Table S2), confirming that group structure does not artifactually result from the bgPCA (52). Indeed, group differences account for a substantial amount of variance (R^2) in the raw shape data, indicating that group separation is not spurious (52), although intergroup variance is increased to a similar extent by the standard bgPCA space and the cross-validated bgPCA (*SI Appendix*, Table S2).

bgPC1 (40.7% of the total variance) pulls apart hominids (mostly positive values) from hylobatids (negative values), with no overlap. Positive values along this axis indicate short and bulgy SCs, together with a right angle between the anterior and posterior SCs. Orangutans and humans display the most extreme condition due to the stoutness of their SCs. Chimpanzees, bonobos, and gorillas show a broad range of variation, with some individuals close to the origin due to their somewhat slenderer SCs (albeit less so than in hylobatids, which display negative values), and others overlapping with *Pongo* and *Homo*. Along bgPC1, *Hispanopithecus* overlaps with australopiths, extant great apes, and humans, while the *Rudapithecus* specimens fall within the African great ape range. Both RUD 77 and RUD 200 closely approach the origin, with the latter showing slightly more positive values. *Oreopithecus* and *Nacholapithecus* are found on moderate negative values, within the lower range of *Pan* and *Gorilla*, due to their quite slender SCs (albeit clearly stouter than in hylobatids).

The patterns of shape variation captured by bgPC2 (33.4% of total variance) (Fig. 3*A*) reflect changes in the shape of three canals as well as their relative proportions. In particular, bgPC2 clearly discriminates *Homo* (with most negative values) from the rest of the sample, due to the presence in the former of a large and rounded (sometimes even slightly superiorly elongated) anterior canal, a posterolaterally displaced inferior portion of the posterior canal, and a small, fairly anterolaterally elongated lateral canal, whose slender portion connects to the vestibule more superiorly and anterolaterally than in apes. The latter fall on intermediate and positive values, with hylobatids considerably overlapping with *Pan* spp. (Fig. 3*A*). To a large extent, this is due to their anterior canal shape, which appears intermediate

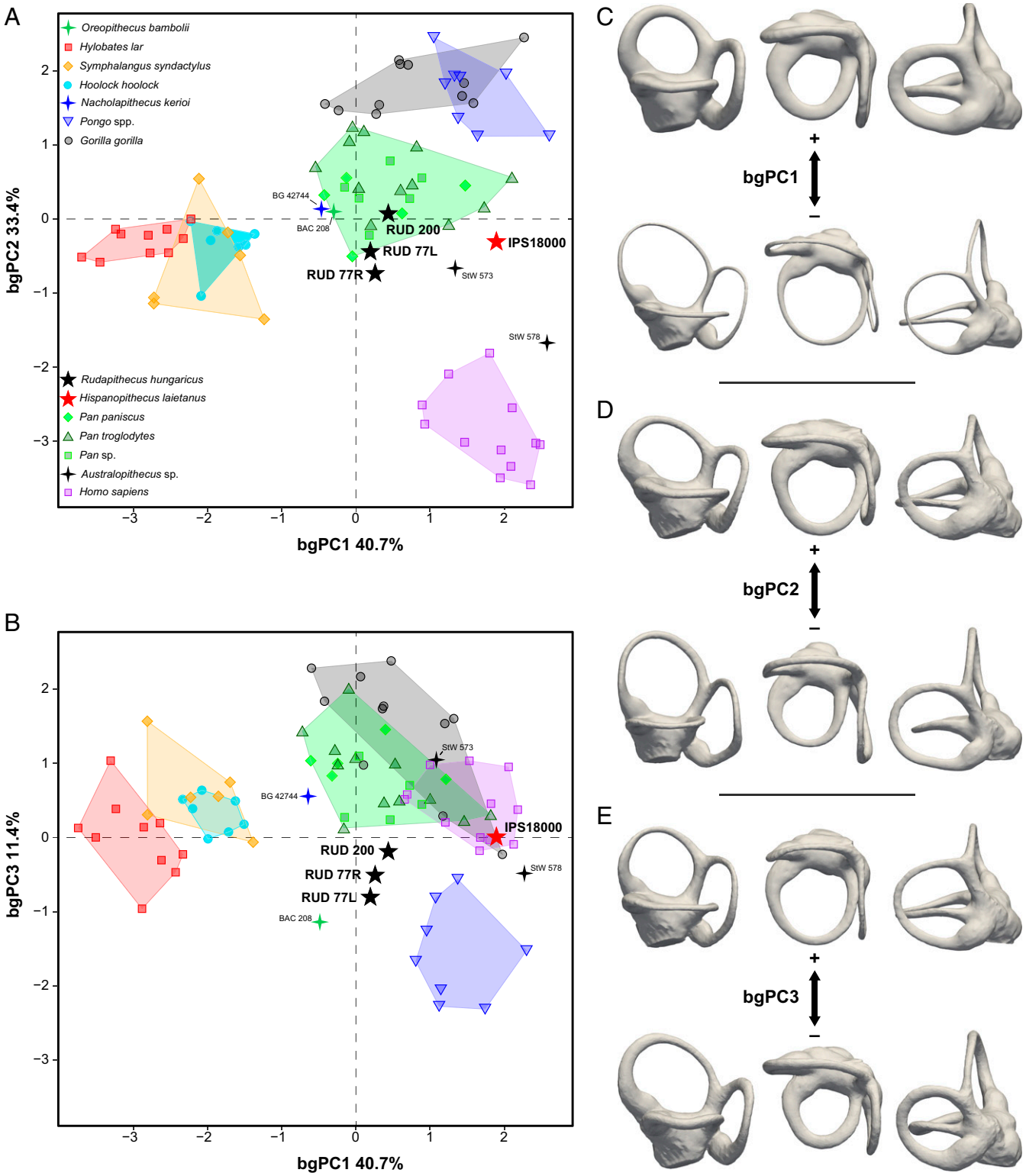

Fig. 3. Results of the bgPCA based on vestibular shape (as reflected by deformation data) in hominoids using genera as grouping factor (variance explained by each bgPC is included within parentheses): (*A*) bgPC2 vs. bgPC1; (*B*) bgPC3 vs. bgPC1. Extreme conformations for each bgPC are displayed: (*C*) bgPC1; (*D*) bgPC2; (*E*) bgPC3. Convex hulls are drawn for each hominoid genus and colored as follows: blue, *Pongo*; black, *Gorilla*; green, *Pan*; lilac, *Homo*; red, *Hylobates*; orange, *Symphalangus*; cyan, *Hoolock*.

between the rounded morphology of humans and the marked vertical compression of *Pongo* and *Gorilla* (the latter taxa occupying more positive values with only very slight overlap with *Pan* and hylobatids). Both *Rudapithecus* and *Hispanopithecus*, like *Oreopithecus* and *Nacholapithecus*, show intermediate values along this axis, overlapping with hylobatids and *Pan* spp. (as well as the *Australopithecus* specimen StW 573), but not with *Pongo* and *Gorilla*. Conversely, the other australopith (StW 578) more closely approaches humans due to its larger vertical SCs.

bgPC3 (11.4% of variance) (Fig. 3*B*) is driven by the shape of the anterior canal, its relative size relative compared with that of the lateral one, the length of the CC, and the amount of torsion of the lateral canal. Thus, negative values reflect a large and anterosuperiorly projecting anterior canal, coupled with a small lateral one, and a short CC. This axis discriminates *Pongo* (most negative values) from the rest of the sample, only minimally overlapping with some *Hylobates*. One individual of *Rudapithecus* (RUD 77) and *Oreopithecus* overlap with the range of orangutans due to their anterosuperiorly projecting anterior canal (albeit less so in RUD 77), short CC, and markedly small lateral canal. A similar morphology of the anterior canal is also found in some *Hylobates* and in one of the *Australopithecus* specimens (StW 573), resulting in moderately negative scores. *Hispanopithecus* and the other individual of *Rudapithecus* (RUD 200) fall at the negative end of the gorilla and human variation, due to their intermediate anterior canal morphology, longer CC (yet less so than in most *Pan* and *Gorilla* individuals), and a larger lateral canal. *Nacholapithecus* and the other australopith specimen (StW 578) fall among moderate positive values, overlapping with gorillas, chimpanzees, bonobos, humans, and hylobatids, due to their long CC and more vertically aligned (i.e., superiorly directed) connection of the anterior canal with the CC.

When the inspected bgPCs are considered simultaneously to compute posterior probabilities of group membership (Table 1), the *Rudapithecus* RUD 77 individual occupies a position in the morphospace that does not fit well with most extant hominoid genera ($P < 0.05$), rather approaching the position of *Nacholapithecus* and *Oreopithecus* in the morphospace (Table 2). Conversely, RUD 200 shows considerable similarities with *Pan* ($P = 0.549$) and *Nacholapithecus*. The three *Rudapithecus* specimens fall closer to one another than either approaches the single specimen of *Hispanopithecus* (Table 2), which is also more distant than *Nacholapithecus* from all the considered specimens (Table 2). *Hispanopithecus* mostly differs along bgPC1, sharing similarities in the volumetric proportions of the SCs and in the vertically compressed anterior canal morphology with *Australopithecus* individual StW 573 (Table 2). IPS18000 marginally differs from *Pan* ($P = 0.053$) and is clearly an outlier compared to the remaining extant genera.

The cluster analyses based on the significant bgPCs (Fig. 4*A*) and raw shape data (Fig. 4*B*) further support the aforementioned results, since *Rudapithecus* and *Hispanopithecus* do not cluster with one another and show affinities with different taxa. In particular, the cluster based on the bgPCA results (Fig. 4*A*) indicates that *Rudapithecus* is most similar to both *Pan* and *Nacholapithecus*, while *Hispanopithecus* approaches hominins. This is further supported by the raw shape data cluster (Fig. 4*B*), which mainly differs by recovering a great ape cluster.

Phylomorphospace and Reconstruction of Ancestral Morphologies. The shape data, as captured by the bgPCA performed on the extant hominoid sample, approaches the Brownian motion model of evolution, as supported by the phylogenetic signal computed for the bgPCs ($K_{mult} = 0.864$, $P = 0.019$) and for the raw data (i.e., the deformation fields; $K_{mult} = 0.863$, $P = 0.017$). We used phylogenetically informed techniques on the shape data to visualize the direction and magnitude of vestibular shape change during hominoid evolution as well as to depict the internal nodes of the phylogeny—that is, the inferred vestibular morphology of the last common ancestors (LCAs) of major groups—as reconstructed by maximum likelihood. The results are very similar irrespective of the precise phylogenetic placement of dryopiths as stem hominines (Fig. 5 and *SI Appendix*, Fig. S2*B*), stem hominids (*SI Appendix*, Figs. S2*A* and S3 *A* and *C*), or stem pongines (*SI Appendix*, Figs. S2*C* and S3 *B* and *D*). The crown hominoid LCA (Figs. 5 and 6*A*) is reconstructed as possessing evenly sized and moderately inflated SCs, a moderately long and not inflated CC, a fairly vertically compressed, yet not anterosuperiorly projecting anterior canal, an almost rounded posterior canal, an obtuse angle between the planes identified by the anterior and posterior canals (close to the right angle), and a right angle among the SCs merging at the CC apex

Table 1. Mahalanobis squared distances (D^2) between fossil scores and extant hominoid group centroids and associated posterior probabilities (P) of group membership for all fossil individuals

D^2 or P	*Hoolock*	*Symphalangus*	*Hylobates*	*Pongo*	*Gorilla*	*Pan*	*Homo*
D^2							
IPS18000 (*Hispanopithecus laietanus*)	6.086	6.861	10.532	9.229	5.329	**1.407**	5.076
RUD 77R (*Rudapithecus hungaricus*)	**2.044**	2.776	4.233	8.831	9.809	2.736	4.063
RUD 77L (*Rudapithecus hungaricus*)	**2.252**	3.325	4.104	6.735	10.091	3.132	5.621
RUD 200 (*Rudapithecus hungaricus*)	2.478	3.312	5.338	7.475	5.174	**0.745**	6.566
BAC 208 (*Oreopithecus bambolii*)	4.359	6.261	4.809	**4.087**	15.042	7.218	11.210
BG 42744 (*Nacholapithecus kerioi*)	1.200	1.662	3.546	10.016	4.942	**0.683**	7.673
StW 573 (*Australopithecus* sp.)	5.323	5.367	9.865	14.341	5.192	**1.246**	4.182
StW 578 (*Australopithecus* sp.)	9.400	10.538	13.134	10.554	16.362	7.661	**2.552**
P							
IPS18000 (*Hispanopithecus laietanus*)	<0.001	<0.001	<0.001	<0.001	<0.001	**0.053**	<0.001
RUD 77R (*Rudapithecus hungaricus*)	0.006	0.003	<0.001	<0.001	<0.001	**0.011**	<0.001
RUD 77L (*Rudapithecus hungaricus*)	**0.015**	0.005	<0.001	<0.001	<0.001	0.012	<0.001
RUD 200 (*Rudapithecus hungaricus*)	<0.001	<0.001	<0.001	<0.001	<0.001	**0.549**	<0.001
BAC 208 (*Oreopithecus bambolii*)	**0.016**	0.001	<0.001	<0.001	<0.001	<0.001	<0.001
BG 42744 (*Nacholapithecus kerioi*)	0.035	0.012	<0.001	<0.001	<0.001	**0.184**	<0.001
StW 573 (*Australopithecus* sp.)	<0.001	<0.001	<0.001	<0.001	<0.001	**0.026**	<0.001
StW 578 (*Australopithecus* sp.)	<0.001	<0.001	<0.001	<0.001	<0.001	<0.001	**0.013**

Note that these are probability estimates of having a particular score given membership in a particular group, not the likelihood of group membership in each of a priori defined groups given a particular score. The lowest D^2 and the highest probability for each specimen are in bold.

Table 2. Mahalanobis distances (D^2) between dryopiths and other fossils

D^2	IPS18000	RUD 77R	RUD 77L	RUD 200
IPS18000 (*Hispanopithecus laietanus*)	—	2.037	2.504	1.012
RUD 77R (*Rudapithecus hungaricus*)	2.037	—	0.179	0.772
RUD 77L (*Rudapithecus hungaricus*)	2.504	0.179	—	0.848
RUD 200 (*Rudapithecus hungaricus*)	1.012	0.772	0.848	—
BAC 208 (*Oreopithecus bambolii*)	6.678	2.495	1.385	3.571
BG 42744 (*Nacholapithecus kerioi*)	2.286	1.270	1.505	0.416
StW 573 (*Australopithecus* sp.)	0.703	2.587	3.657	1.637
StW 578 (*Australopithecus* sp.)	3.080	2.745	3.087	4.479

These distances are based on the scores of the significant bgPCs (bgPC1 – bgPC3).

(Fig. 6*A*). Irrespective of the phylogenetic assumptions for dryopiths, the reconstructed LCA for crown hominoids is closer to hominids (especially *Nacholapithecus*, *Rudapithecus* and, among extant taxa, *Pan*) than to hylobatids (Fig. 5), in terms of their intermediate volumetric proportions, contrasting with the markedly slenderer SCs of gibbons and siamangs. In turn, the LCAs of crown hominines and dryopiths (*Rudapithecus* + *Hispanopithecus*) closely resemble one another irrespective of the underlying phylogenetic assumptions for the fossil species (Fig. 5 and *SI Appendix*, Fig. S3), being extant hominid-like in volumetric proportions but otherwise showing a more plesiomorphic morphology in the evenly sized and fairly rounded SCs.

The inferred LCA of crown hominids, in particular, closely resembles that of crown hominoids, except for the stouter volumetric proportions, more derived toward the extant hominid condition (Figs. 5 and 6*B*). It displays equally sized SCs, an obtuse to right angle in the apex of a moderately long CC, and a slightly laterally elongated posterior canal (Fig. 6*B*). Orangutans appear derived from the LCA by displaying more inflated SCs (especially the anterior one) (Figs. 1*J* and 6*B*), further diverging in the opposite direction from African great apes and humans because its short and extremely stout CC, as well as its anterosuperiorly projecting anterior canal and marked torsion of the lateral canal (Fig. 5*B*). The LCA of hominines (Fig. 6*C*) appears somewhat more derived than the LCAs of hominoids and hominids for both volumetric proportions and SC shape. It displays moderately stout SCs and medium/large vestibular recesses, equally developed SCs (with a slightly smaller lateral one), a vertically compressed anterior canal (more so than in any other LCA), a slightly laterally projecting posterior canal, and a long CC with an obtuse angle in its apex (Fig. 6*C*). *Homo* and *Gorilla* would have evolved in opposite directions from this ancestral morphology in terms of SC relative size, with humans showing the largest vertical canals (Figs. 1*M* and 5*A*) and gorillas displaying a larger lateral canal (Figs. 1*K* and 5*A*). Chimpanzees and bonobos, due to their equally sized SCs and fairly elongated CC (Figs. 1*L* and 5*A*), are closer to the hominine LCA morphology, while *Australopithecus* appears derived toward the human condition, due to the moderate increase in the size of the anterior and posterior canals (Fig. 5). The reconstructed morphotype for the LCA of the investigated dryopiths (Fig. 6*D*) closely resembles those of hominines and hominids by displaying moderately stout and evenly sized SCs (with a slightly smaller lateral one), an obtuse angle at the CC apex, and a not anterosuperiorly projecting anterior canal, differing from the hominid LCA by the somewhat less vertically compressed anterior canal (Fig. 6 *B* and *D*).

Hispanopithecus and *Rudapithecus* appear to have diverged in opposite directions from their LCA (Fig. 5). The former seems derived in the volumetric proportions (similarly to *Pongo*, *Australopithecus*, and *Homo*), whereas the *Rudapithecus* condition in this regard is very similar to that of *Pan* as well as the reconstructed hominid LCA, and (to a lesser extent) to those of *Nacholapithecus* and *Oreopithecus* (Figs. 5 and 6*B*). Similarly, the fairly short CC and a somewhat anterosuperiorly projecting anterior canal found in *Rudapithecus* (less so than in orangutans and *Oreopithecus*) contrast with the longer CC and the rectangular-shaped anterior canal found in *Hispanopithecus* (Fig. 1*D*). In these regards, *Hispanopithecus* more closely resembles the members of the African ape and human clade (Fig. 1 *A*–*C*).

In summary, each extant hominid genus is derived in a particular direction from the ancestral morphology, with *Pan* remaining close to the hominid and hominine LCAs;

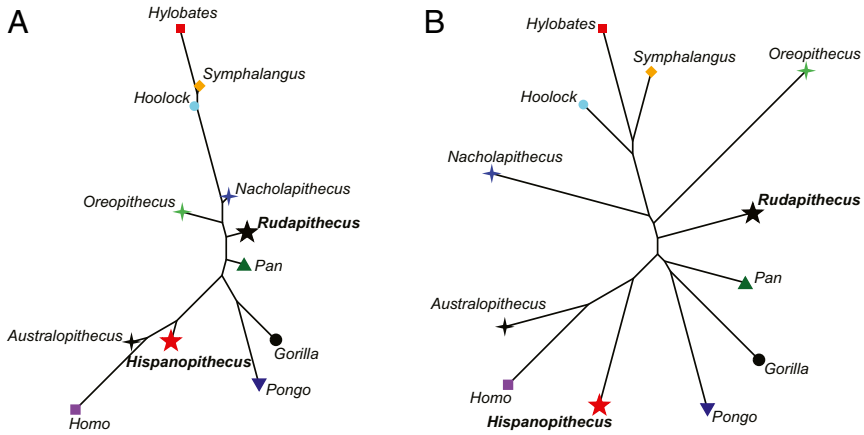

Fig. 4. Dendrograms resulting from neighbor joining cluster analyses based on: (*A*) The weighted Euclidean distances computed for the bgPCs (cophenetic correlation: 0.98); (*B*) the Euclidean distances computed for the raw shape data (i.e., the deformation fields) obtained from the deformation-based 3DGM analysis (cophenetic correlation: 0.96).

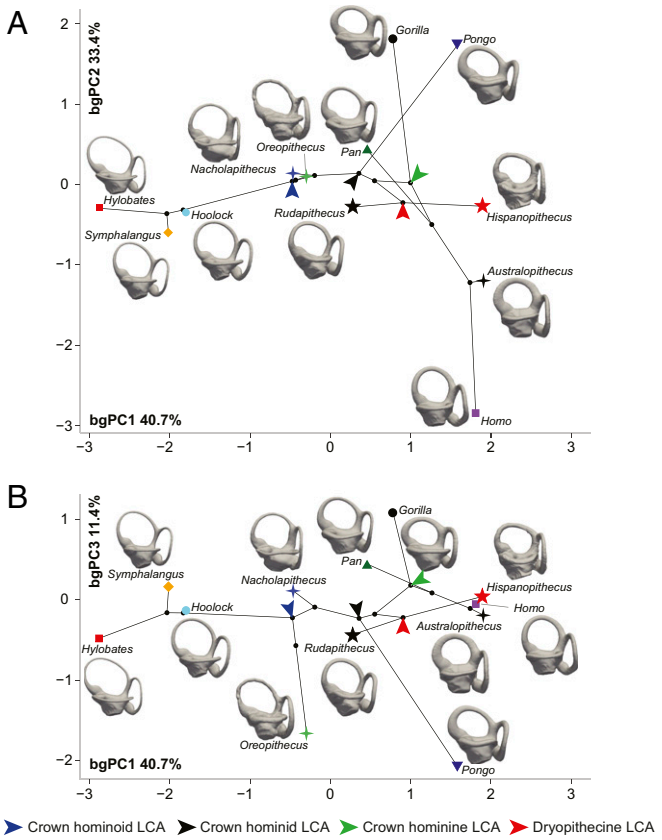

Fig. 5. Phylomorphospaces of the vestibular apparatus in hominoids, obtained by projecting the phylogenetic tree that considers dryopithecines a clade of stem hominines (*SI Appendix*, Fig. S1*B*) on bivariate plots between bgPCs. The tips correspond to genus bgPCA score centroids: (*A*) bgPC2 vs. bgPC1; (*B*) bgPC3 vs. bgPC1. Key ancestral morphologies reconstructed using maximum likelihood for the LCAs of various clades are depicted by means of arrowheads. See *SI Appendix*, Fig. S2 for the results based on alternative phylogenetic hypotheses (*SI Appendix*, Fig. S1 *A* and *C*).

Nacholapithecus appears as the least derived among both extant and fossil hominid taxa, together with *Oreopithecus.* The latter taxon also shows similarities with *Pongo* in the anterosuperiorly projecting anterior canal (Fig. 1 *E* and *J*), despite being much slenderer in *Oreopithecus*. Overall, the dryopiths appear less derived than most extant genera relative to either the crown hominid or the crown hominine LCA, irrespective of their preferred phylogenetic placement. *Rudapithecus* appears more primitive than *Hispanopithecus*, being closer than the latter to both *Nacholapithecus* and *Oreopithecus,* and closely approaching both the reconstructed crown hominid LCA and *Pan* (Figs. 1, 5, and 6). In contrast, *Hispanopithecus* is in some respects more derived than *Rudapithecus*, particularly toward orangutans, australopiths, and humans in the large vestibular recesses and in the stout SC volumetric proportions, and toward orangutans alone in the rounded posterior canal morphology (Fig. 5). Despite *Hispanopithecus* sharing its CC apex morphology (intermediate between African great apes and orangutans) and anterior canal shape (not anterosuperiorly projecting, yet not as squared as in gorillas) with *Homo* and *Australopithecus*, this condition could be plesiomorphic for hominids as a whole, as it is also found in the stem hominid *Nacholapithecus* (Fig. 5). Overall, the two dryopiths share with African great apes and humans some features (moderately stout SCs, not anterosuperiorly projecting the anterior canal, fairly long CC), but according to our analyses these features appear primitive (being likely present in the hominid LCA and, to a lesser extent, *Nacholapithecus*), with hominines (particularly gorillas) and especially orangutans having subsequently derived in opposite directions.

Discussion

Our results show that the vestibular morphology of both *Hispanopithecus* and *Rudapithecus* more closely resembles that of extant great apes and humans than that of hylobatids, in agreement with the current consensus that they belong to the great-ape-and-human clade (2, 3, 6, 26). These similarities particularly concern the volumetric proportions of the SCs as well as the size of the latter relative to the vestibular recesses. Volumetric proportions, as reflected by the ratio between the volume and the length of the SCs, appear particularly relevant given that an allometric grade shift has been previously identified to characterize all extant hominids, so that they display relatively more voluminous SCs than other anthropoids (including hylobatids) at comparable

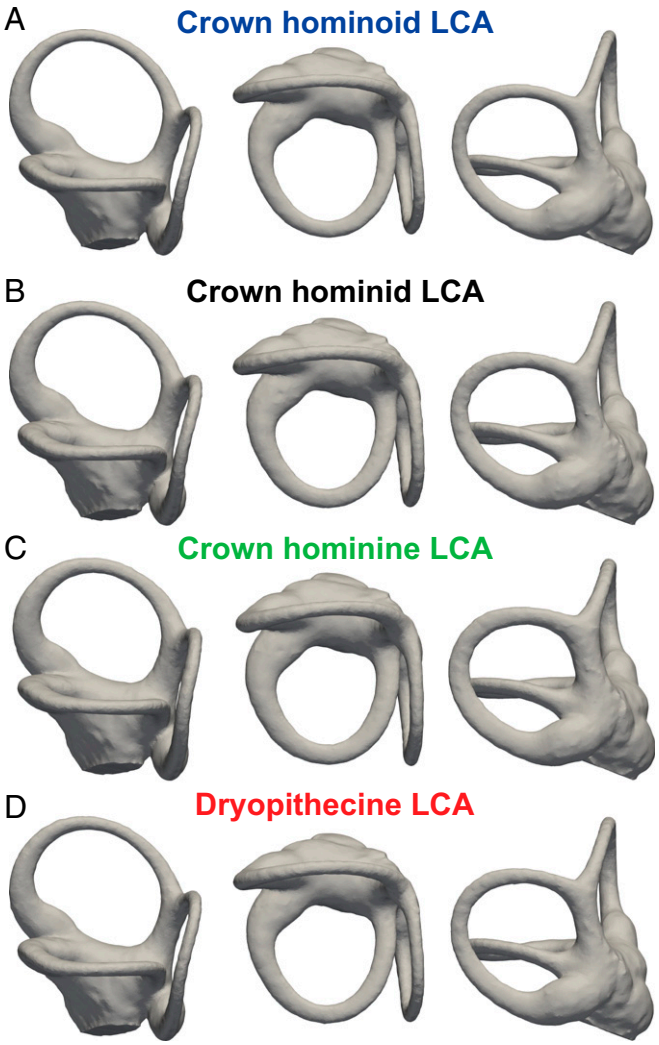

Fig. 6. Reconstructed vestibular shape for the LCA of the main clades of interest as inferred using maximum-likelihood methods for deformation-based 3DGM analyses applied to the hominoid sample under the stem-hominine phylogenetic hypothesis for dryopiths (*SI Appendix*, Fig. S1*B*), in posterolateral (*Left*), superior (*Center*), and posteromedial (*Right*) views. The reconstructed LCAs depicted are the following: (*A*) Crown hominoids; (*B*) crown hominids; (*C*) crown hominines; (*D*) dryopithecines (*Hispanopithecus* + *Rudapithecus*). The results for the other phylogenetic hypotheses (not shown) are virtually identical.

lengths (5). The derived condition of hominids has been linked with locomotion (5), but is noteworthy that chimpanzees, bonobos, and gorillas are slightly more variable in SC volumetric proportions than orangutans and humans. Given the relationship between SC shape variation and locomotion noted by some authors (53, 54), our results might reflect stronger locomotor-related selection pressures in orangutans and humans.

The classification results based on the bgPCA as well as the cluster analyses indicate that the two investigated dryopiths are distinguishable from one another, with the three specimens (two individuals) of *Rudapithecus* being more similar to one another than to the single specimen of *Hispanopithecus*. This result, together with other cranial differences (e.g., morphology of the frontal squama, premaxilla, and zygomatic), supports the distinction of these taxa at the genus rank (2, 3, 7, 21, 25, 35). *Rudapithecus* generally displays a somewhat more primitive morphology, closer to the one inferred for the crown hominid LCA. It shows some similarities with the fossil hominoids *Oreopithecus* and *Nacholapithecus*. The latter taxon appears more primitive than other hominids, in agreement with a previous study based on the entire inner ear morphology (49). However, both the hominid-like volumetric proportions of *Nacholapithecus* and the lack of a subarcuate fossa (55) support its stem hominid status, closely resembling the morphotype reconstructed for the crown hominid LCA. The morphology of *Rudapithecus* also resembles that of crown hominids, such as *Pan* (volumetric proportions and the relative size of the SCs) and, to a lesser extent, orangutans (the somewhat anterosuperiorly projecting anterior canal and the short CC). As previously noted (5), chimpanzees and bonobos appear least derived than other extant hominids. This is shown by the possession of similarly sized SCs (shared with the reconstructed crown hominid and crown hominine LCAs, while the dryopith LCA displays a slightly smaller lateral canal) and, especially, by the fairly slender volumetric proportions (intermediate between the hominine and hominid LCAs, yet closer to the latter). This is also supported by the similarities between *Pan* species and Miocene apes, especially *Nacholapithecus*. Nonetheless, chimpanzees and bonobos appear derived in some features (the small and rounded posterior canal as well as the obtuse angle of the CC apex), just like gorillas and humans are derived in other directions (largest lateral canal relative to the other SCs and markedly enlarged vertical canals, respectively).

Among hominids, orangutans and humans show the most extreme condition in the volumetric proportions of the SCs. Orangutans further diverge from the hominid LCA by the anterosuperiorly projecting anterior canal (even more so than in hylobatids). *Hispanopithecus* appears more derived than the other Miocene taxa, especially by the stouter SCs, while it does not fit well within the variation of any extant genus. More clearly than *Rudapithecus*, *Hispanopithecus* displays a mosaic of features that is unknown among extant hominids, including similarities with chimpanzees and bonobos (in the long CC), humans (the obtuse angle of the CC apex and the right angle between the planes of the posterior and lateral canals), and orangutans (the stout CC and the voluminous vestibular recesses, the latter also shared with humans) coupled with some unique features (the swollen area between the ampulla and the tip of the lateral canal, and the markedly inflated ampullae).

Interpreting the similarities of the investigated dryopiths in evolutionary terms is not straightforward. The results of the phylomorphospace approach and the reconstructed ancestral vestibular morphologies suggest that modern hominid-like volumetric proportions of the SCs would have been present in the LCA of crown hominids, while that of crown hominoids as a whole would have displayed somewhat intermediate proportions between hylobatids and hominids (yet closer to the latter). Differences in volumetric proportions of the SCs have been related to locomotor adaptations, because they directly affect the sensitivity and steadiness of the SCs in response to angular accelerations (5, 56). Hence, the moderately stout SCs of the LCA of crown hominids indicate that it showed a slow type of locomotion, which was present, to a large extent, also in the LCA of crown hominoids, as previously inferred based on the size of the SC radius alone (41). Both *Rudapithecus* and *Hispanopithecus* show a wide gap between the lateral and posterior canals (the planes defined by them are well separated and do not intersect), caused by the anterolateral location of the lateral canal. This trait has been linked to orthograde behaviors (42), in agreement with the fossil evidence available for these taxa (6, 11, 23, 25, 35, 57–61). However, from a phylogenetic viewpoint, the presence of the aforementioned feature in the investigated dryopiths is less informative than their hominid-like volumetric proportions, since the former have been identified as a synapomorphy of crown hominoids as a whole (5).

We conclude that, with differences that are consistent with their distinction at the genus rank, both *Hispanopithecus* and *Rudapithecus* display a unique hominid-like vestibular morphology that differs from that of any extant hominid genera but that appears quite close to that ancestral for crown hominids and crown hominines, mainly diverging from that of hylobatids by the stouter volumetric proportions of the SCs that are uniquely characteristic of great apes and humans among anthropoids. Orangutans appear most derived from such an ancestral vestibular morphology, whereas the investigated dryopiths lack most orangutan-like derived features, except for the slightly anterosuperiorly projecting anterior canal in *Rudapithecus* (also found in *Hylobates*) and some torsion in the shape of the lateral canal (a character that appears to be quite variable within hominoids). The lack of orangutan-derived features in dryopithecines does not completely rule out a stem pongine status, as previously supported by some authors (10, 28, 29), as it represents a more primitive morphology that probably precedes the subsequent evolution of the orangutan-like features in the pongine lineage. However, our results are more consistent with a stem hominid (6, 30) or a stem hominine (2, 3, 14, 16, 25) status for the investigated dryopiths. Our results suggest that African apes and hominin genera evolved in different directions from an ancestral morphology that more closely resembles that of *Pan* among extant hominines, and which is largely plesiomorphic for hominids, as further supported by similarities with the stem hominid *Nacholapithecus* (except for the slenderer volumetric proportions of the latter). Therefore, similarities between the SC morphology of the studied dryopiths and that of African apes do not necessarily imply a hominine status, but overall support the previous claim (5), based on extant taxa alone, that extant hominines evolved from an ancestral condition quite similar to that of the crown hominid LCA, and that the latter was characterized by derived volumetric proportions of the SCs. Pending the analysis of other Miocene apes, *Pan* among the extant taxa and *Rudapithecus* among extinct apes constitute the best available proxies for such ancestral morphologies, being already somewhat more derived from the crown hominoid condition that is best approximated by *Nacholapithecus*. In the future, the inclusion in the analyses of additional extinct hominoids will hopefully clarify further the evolutionary history of these hominoids during the Miocene.

Materials and Methods

Sample Composition and Acquisition. We inspected three petrosals from two individuals of *R. hungaricus* from Rudabánya, Hungary (RUD 77, left [RUD 77L] and right [RUD 77R]; and RUD 200, right) (12, 13) and the single available petrosal of *H. laietanus* from Can Llobateres 2, Spain (IPS18000, right) (10, 28, 29). The specimens of *Rudapithecus* are housed at the Geological Museum of the Mining and Geological Survey of Hungary and were scanned with a Skyscan 1172 (obtaining a resolution of 0.0136 mm) at the

Max Plank Institute for Evolutionary Anthropology (Leipzig, Germany), with the following parameters: 100-kV voltage and 100 mA. In turn, IPS18000 is housed at the Institut Català de Paleontologia Miquel Crusafont in Sabadell (Spain) and was scanned with a GE Phoenix V|Tome|X s 240 (obtaining a resolution of 0.0295 mm) at the Centro Nacional de Investigación sobre la Evolución Humana (Burgos, Spain), with the following parameters: 125-kV voltage and 120 mA. The three-dimensional (3D) virtual models of IPS18000, RUD 200 and RUD 77R were mirrored to enable the comparison with extant species. The segmented surfaces of the SCs of these fossils are available from MorphoSource (https://www.morphosource.org) (*SI Appendix*, Table S3).

The comparative sample for the volumetric proportion evaluation has been taken from a previous analysis that evaluated the phylogenetic signal embedded in the vestibule morphology (5), and integrated with recently published material of extant hominoids (4) and humans (62), together with the stem hominid *N. kerioi* (49). Overall, it consists of μCT scans of 169 dried crania and petrosals belonging to 27 extant anthropoid species, including all hominid genera and a selection of hylobatids, cercopithecoids, and platyrrhines, together with fossil taxa (*SI Appendix*, Table S3). The 3D meshes of the inner ear bony labyrinth of StW 573 and StW 578 were downloaded from the Sterkfontein project of the digital repository http://MorphoSource.org. The juvenile status of a few specimens should not affect their vestibular morphology since the bony labyrinth ossifies in early prenatal stages and does not change subsequently (63). The analysis of the patterns of shape variation was focused on hominoids alone and was based on a subsample of 77 individuals representing all extant hominoid genera (*SI Appendix*, Table S4). Part of the scans used in the study originally appeared in refs. 64 and 65.

The μCT scans (voxel size for the extant and fossil specimens added in the present analysis to those originally published in ref. 5 can be found in *SI Appendix*, Table S4) were segmented using Avizo 9.0.1 (FEI Visualization Sciences Group) to digitally extract the left bony labyrinth, when available, or that from the right side (mirrored before the surface alignment). The vestibular apparatus was separated from the cochlea by cutting the generated 3D surfaces right under the saccule and the oval window and filling the resulting holes with Geomagic Studio 2014 (3D Systems) using a flat surface (5).

The anatomical axes used for describing SC morphology corresponds to those employed in the vast majority of inner ear analysis focusing on primates (36, 37, 42, 49), which conventionally follow the same orientation as in humans (i.e., superior/inferior and anterior/posterior).

Shape Analysis. Shape was analyzed using a deformation-based 3DGM technique that does not rely on a priori defined landmarks and examines the geometrical correspondences between continuous surfaces (5, 48, 66–68). This method quantifies the deformation from the analyzed surfaces from a constructed sample-average surface (template) (66, 68), mathematically models them as a diffeomorphism, and computes a set of vectors (momenta) that describe the direction and magnitude of deformation from the average template. The unscaled 3D models were aligned with Avizo 9.0.1 using the "Align Surface" module before running the analyses. The diffeomorphisms and the momenta were computed in the Barcelona Supercomputing Center (Barcelona, Spain) with Deformetrica 4 software. The 3D models of the fossils were projected a posteriori in the tangent space generated by means of bgPCA ran on the set of momenta for the hominoid-only sample using genera as grouping factor. The bgPCA was computed in R Studio v1.1.453 for R v3.5.0 using the *ade4* package (69), while the cross-validated bgPCA was derived using the "groupPCA" function of the *Morpho* v2.6 (70) library. Group mean differences were tested by computing a permutational ANOVA (1,000 permutations) based on the Euclidean distance between the means using the "adonis" function of the *Vegan* package (71). The amount of variance (R^2) explained by group differences in the raw shape data, and in the scores of both standard and cross-validated bgPCA results, was estimated with the same function as for the permutation test. To further assess similarities between the analyzed fossil taxa and extant hominoid genera in terms of vestibular morphology, we computed Mahalanobis squared distances (D^2) between the bgPC scores of fossils and group centroids used in the bgPCA. The distances were also used to compute the posterior probabilities of group membership for the fossil specimens by means of the "typprobClass" function of the *Morpho* v2.6 (70) package, on the basis of the multivariate normal distribution of extant groups defined a priori in the bgPCA analyses. The similarities between extant and fossil hominoids were further investigated by means of a cluster analysis (neighbor joining) computed using the "nj" function of the *ape v5.3* package in R (72) on the basis of species mean configurations for the raw data and of weighted Euclidean distances between pairs of species bgPC centroid scores, obtained using the "distances" function of the *distances* v0.1.8 package in R (73)

Additionally, the correlation between the log-transformed cube root of SC volume (ln VolSC, in millimeters) and log-transformed SC length (ln L, in millimeters) was assessed means of ordinary least-squares linear regression, as the relationship between these variables has previously been shown to display an allometric grade shift between hominids and other anthropoids (5). Two separate regressions were computed for the nonhominid anthropoids and for great apes and humans using SPSS Statistics v. 17.0 for Windows (see figure 7b in ref. 5). The regression for the nonhominid sample was used as a baseline for computing the allometric residuals (*SI Appendix*, Table S1) (see table 5 in ref. 5) for the extant and extinct species. Comparisons between the latter and extant groups are depicted by means of box-and-whisker plots.

Phylomorphospace and Phylogenetic Signal. Major patterns of vestibular shape variation were quantified using a phylomorphospace approach (74), obtained by projecting a phylogeny on to the tangent space derived from the bgPCA of a 3DGM shape analysis. In this method, the tips of the phylogeny correspond to the genus bgPC centroid, while the internal nodes (i.e., the ancestral states) of the tree are estimated using a maximum-likelihood method for continuous characters, assuming that the reconstructed nodes approximate the true morphology of the ancestors. Thus, when a time-calibrated phylogeny is used, its two-dimensional representation enables the intuitive interpretation of the magnitude and direction of evolution, based on branch length and orientation. The molecular-based phylogenetic tree for extant hominoids used in this analysis was downloaded from the 10kTrees Website (v3; https://10ktrees.fas.harvard.edu/), while *Hispanopithecus* and *Rudapithecus* were added based on the assumption that they are closely related and constitute a clade, with the tips corresponding to 9.6 Ma and 10.1 Ma, respectively (20), and diverging at 11.1 Ma, but considering three different phylogenetic placements for these taxa as discussed in the literature during the last two decades (see above): stem hominids, stem hominines, and stem pongines (*SI Appendix*, Fig. S2). Analyses were repeated based on the resulting three different cladograms and their results compared to evaluate the effect of phylogenetic uncertainties surrounding these taxa. *Oreopithecus* is here considered as a stem hominoid as indicated by most recent cladistic analyses (4). *Nacholapithecus* has been included in a stem hominid position, 2 Myr older than the divergence between pongines and hominines (crown hominids), thus always preceding the divergence of dryopiths in all the phylogenetic hypotheses, and its tip corresponds to 14.77 Ma (55, 75). The divergence between crown hominoids and *Oreopithecus* has been placed 1 Myr older than the divergence between hylobatids and hominids and its tip corresponds to its last occurrence in the fossil record (7.0 to 6.5 Ma) (76). For the South African *Australopithecus* sp., we used the published first appearance datum for *Australopithecus africanus* (4.02 Ma) that includes the Jacovec specimens into the species (77).

The position in the morphospace of the internal nodes of the phylogeny (ancestral morphologies) was estimated via a maximum-likelihood method for continuous characters (78) using the "fastAnc" function of *phytools* v0.6-60 R package (79). Subsequently, the bgPC scores of the ancestral states were rotated and translated from the shape data back into the configuration space for interpolation and 3D visualization using Deformetrica 3 software.

The phylogenetic signal embedded in vestibular shape, as captured by all the bgPCs, was quantified by means of the multivariate phylogenetic index K_{mult} (80) using *geomorph* v3.1.1 (81) R package. The K_{mult} statistic, like its univariate counterpart (82), assesses the amount of phylogenetic signal relative to that expected for character undergoing Brownian motion and reflects the accuracy with which the phylogenetic tree describes the variance–covariance pattern found in the shape data. It is also informative about the accumulation of the variance in the phylogeny. Thus, $K_{mult} \sim 1$ is obtained when the inspected mode of evolution can adequately be described using a stochastic Brownian motion model. For $K_{mult} < 1$, the majority of the variance is found within clades, thus implying that neighbor taxa resemble one another less than expected and that the mode of evolution is not aleatory, possibly as the results of homoplastic adaptations (i.e., related to function rather than phylogeny). Values of $K_{mult} > 1$ indicate that variance is mostly found among different clades, being obtained when close taxa are less diverse that expected under Brownian motion (suggesting that phenomena of stabilizing selection might have occurred).

Data Availability. The 3D mesh data have been deposited in MorphoSource, https://morphosource.org/ (Rudapithecus hungaricus: RUD:77 R: https://doi.org/10.17602/M2/M126214; RUD:77 L: https://doi.org/10.17602/M2/M126215; RUD:200: https://doi.org/10.17602/M2/M126216; Hispanopithecus laietanus: IPS:18000: https://doi.org/10.17602/M2/M126217; Nacholapithecus kerioi:

KNM:BG:42744: https://doi.org/10.17602/M2/M166427; Oreopithecus bambolii: NMB:BAC:208: https://doi.org/10.17602/M2/M166428).

ACKNOWLEDGMENTS. We thank Jose Braga for allowing us to use the CT scans of the human specimens; the Max Plank Institute for providing access to the microCT scans of RUD 77 and RUD 200; the European Synchrotron Radiation Facility heritage database for palaeontology, evolutionary biology, and archaeology, for providing access to a part of the hominoid scans used in the present analysis; and Lynn Copes, Lynn Lucas, and the Museum of Comparative Zoology (Cambridge, MA) for providing access to a part of the scans used in the study, and funded by NSF DDIG #0925793, and a Wenner-Gren Foundation Dissertation Grant #8102 (both to Lynn Copes). These scans were downloaded from MorphoSource.org, a web-accessible archive for three-dimensional digital data housed by Duke University. This research has been funded by the Agencia Estatal de Investigación CGL2016-76431-P and CGL2017-82654-P, AEI/FEDER EU; and BES-2015-071318 (to A.U.); the Generalitat de Catalunya (CERCA Programme); the consolidated research groups 2017 SGR 86 and 2017 SGR 116 GRC; and the French Centre National de la Recherche Scientifique. Part of the analyses were performed using Barcelona Supercomputing Center resources (BCV-2020-1-0008). A.B. was funded by the University of the Witwatersrand.

1. N. J. Stevens *et al*., Palaeontological evidence for an Oligocene divergence between Old World monkeys and apes. *Nature* **497**, 611–614 (2013).
2. D. R. Begun, "The Miocene hominoid radiation" in *A Companion to Paleoanthropology*, D. R. Begun, Ed. (Blackwell Publishing, 2013), pp. 398–416.
3. D. R. Begun, "Fossil record of Miocene hominoids" in *Handbook of Paleoanthropology*, W. Henke, I. Tattersall, Eds. (Springer, ed. 2, 2015), pp. 1261–1332.
4. I. Nengo *et al*., New infant cranium from the African Miocene sheds light on ape evolution. *Nature* **548**, 169–174 (2017).
5. A. Urciuoli *et al*., The evolution of the vestibular apparatus in apes and humans. *eLife* **9**, e51261 (2020).
6. D. M. Alba, Fossil apes from the Vallès-Penedès Basin. *Evol. Anthropol.* **21**, 254–269 (2012).
7. D. R. Begun, Miocene hominids and the origins of the African apes and humans. *Annu. Rev. Anthropol.* **39**, 67–84 (2010).
8. J. Kelley, "The hominoid radiation in Asia" in *The Primate Fossil Record*, W. C. Hartwig, Ed. (Cambridge University Press, 2002), pp. 369–384.
9. P. Andrews, T. Harrison, E. Delson, R. L. Bernor, L. Martin, "Distribution and biochronology of European and Southwest Asian Miocene catarrhines" in *The Evolution of Western Eurasian Neogene Mammal Faunas*, R. L. Bernor, V. Fahlbusch, H.-W. Mittmann, Eds. (Columbia University Press, 1996), pp. 168–207.
10. S. M. Solà, M. Köhler, Recent discoveries of *Dryopithecus* shed new light on evolution of great apes. *Nature* **365**, 543–545 (1993).
11. S. Moyà-Solà, M. Köhler, A *Dryopithecus* skeleton and the origins of great-ape locomotion. *Nature* **379**, 156–159 (1996).
12. L. Kordos, D. R. Begun, A new reconstruction of RUD 77, a partial cranium of *Dryopithecus brancoi* from Rudabánya, Hungary. *Am. J. Phys. Anthropol.* **103**, 277–294 (1997).
13. L. Kordos, D. R. Begun, A new cranium of *Dryopithecus* from Rudabánya, Hungary. *J. Hum. Evol.* **41**, 689–700 (2001).
14. D. R. Begun, C. V. Ward, M. D. Rose, "Events in hominoid evolution" in *Function, Phylogeny and Fossils: Miocene Hominoid Evolution and Adaptation*, D. R. Begun, C. V. Ward, M. D. Rose, Eds. (Plenum Press, 1997), pp. 389–415.
15. D. R. Begun, "African and Eurasian Miocene hominoids and the origins of the Hominidae" in *Hominoid Evolution and Environmental Change in the Neogene of Europe, Vol 2. Phylogeny of the Neogene Hominoid Primates of Eurasia*, L. D. Bonis, G. Koufos, P. Andrews, Eds. (Cambridge University Press, 2001), pp. 231–253.
16. D. R. Begun, "European hominoids" in *The Primate Fossil Record*, W. Hartwig, Ed. (Cambridge University Press, 2002), pp. 339–368.
17. S. Moyà-Solà, M. Köhler, D. M. Alba, I. Casanovas-Vilar, J. Galindo, *Pierolapithecus catalaunicus*, a new Middle Miocene great ape from Spain. *Science* **306**, 1339–1344 (2004).
18. S. Moyà-Solà *et al*., First partial face and upper dentition of the middle Miocene hominoid *Dryopithecus fontani* from Abocador de Can Mata (Vallès-Penedès Basin, Catalonia, NE Spain): Taxonomic and phylogenetic implications. *Am. J. Phys. Anthropol.* **139**, 126–145 (2009).
19. S. Moyà-Solà *et al*., A unique Middle Miocene European hominoid and the origins of the great ape and human clade. *Proc. Natl. Acad. Sci. U.S.A.* **106**, 9601–9606 (2009).
20. I. Casanovas-Vilar, D. M. Alba, M. Garcés, J. M. Robles, S. Moyà-Solà, Updated chronology for the Miocene hominoid radiation in Western Eurasia. *Proc. Natl. Acad. Sci. U.S.A.* **108**, 5554–5559 (2011).
21. D. R. Begun, Dryopithecins, Darwin, de Bonis, and the European origin of the African apes and human clade. *Geodiversitas* **31**, 789–816 (2009).
22. D. M. Alba *et al*., New dental remains of *Hispanopithecus laietanus* (primates: Hominidae) from Can Llobateres 1 and the taxonomy of late Miocene hominoids from the Vallès-Penedès Basin (NE Iberian Peninsula). *J. Hum. Evol.* **63**, 231–246 (2012).
23. D. M. Alba, S. Almécija, I. Casanovas-Vilar, J. M. Méndez, S. Moyà-Solà, A partial skeleton of the fossil great ape *Hispanopithecus laietanus* from Can Feu and the mosaic evolution of crown-hominoid positional behaviors. *PLoS One* **7**, e39617 (2012).
24. D. R. Begun, *Sivapithecus* is east and *Dryopithecus* is west, and never the twain shall meet. *Anthropol. Sci.* **113**, 53–64 (2005).
25. D. R. Begun, M. C. Nargolwalla, L. Kordos, European Miocene hominids and the origin of the African ape and human clade. *Evol. Anthropol.* **21**, 10–23 (2012).
26. P. Andrews, Last common ancestor of apes and humans: Morphology and environment. *Folia Primatol. (Basel)* **91**, 122–148 (2020).
27. M. Böhme *et al*., A new Miocene ape and locomotion in the ancestor of great apes and humans. *Nature* **575**, 489–493 (2019).
28. M. Köhler, S. Moyà-Solà, D. M. Alba, "Eurasian hominoid evolution in the light of recent *Dryopithecus* findings" in *Hominoid Evolution and Environmental Change in the Neogene of Europe, Vol 2. Phylogeny of the Neogene Hominoid Primates of Eurasia*, L. D. Bonis, G. Koufos, P. Andrews, Eds. (Cambridge University Press, 2001), pp. 192–212.
29. S. Moyà-Solà, M. Köhler, New partial cranium of *Dryopithecus* Lartet, 1863 (Hominoidea, primates) from the upper Miocene of Can Llobateres, Barcelona, Spain. *J. Hum. Evol.* **29**, 101–139 (1995).
30. D. M. Alba *et al*., Miocene small-bodied ape from Eurasia sheds light on hominoid evolution. *Science* **350**, aab2625 (2015).
31. D. R. Begun, L. Kordos, "Phyletic affinities and functional convergence in *Dryopithecus* and other Miocene and living hominids." in *Function, Phylogeny, and Fossils: Miocene Hominoid Evolution and Adaptions*, D.R. Begun, C.V. Ward, M.D. Rose, Eds. (Plenum Press, 1997), pp. 291–316.
32. D. R. Begun, How to identify (as opposed to define) a homoplasy: Examples from fossil and living great apes. *J. Hum. Evol.* **52**, 559–572 (2007).
33. S. G. Larson, Parallel evolution in the hominoid trunk and forelimb. *Evol. Anthropol.* **6**, 87–99 (1998).
34. T. C. Rae, Mosaic evolution in the origin of the Hominoidea. *Folia Primatol. (Basel)* **70**, 125–135 (1999).
35. C. V. Ward, "Postcranial and locomotor adaptations of hominoids" in *Handbook of Paleoanthropology*, W. Henke, I. Tattersall, Eds. (Springer, 2015), pp. 1363–1386.
36. F. Spoor, B. Wood, F. Zonneveld, Implications of early hominid labyrinthine morphology for evolution of human bipedal locomotion. *Nature* **369**, 645–648 (1994).
37. F. Spoor, F. Zonneveld, Comparative review of the human bony labyrinth. *Am. J. Phys. Anthropol.* **41**, 211–251 (1998).
38. F. Spoor *et al*., The primate semicircular canal system and locomotion. *Proc. Natl. Acad. Sci. U.S.A.* **104**, 10808–10812 (2007).
39. R. David *et al*., Motion from the past. A new method to infer vestibular apparatus capacities of extinct species. *C. R. Palevol* **9**, 397–410 (2010).
40. R. David, A. Stoessel, A. Berthoz, F. Spoor, D. Bennequin, Assessing morphology and function of the semicircular duct system: Introducing new in-situ visualization and software toolbox. *Sci. Rep.* **6**, 32772 (2016).
41. T. M. Ryan *et al*., Evolution of locomotion in Anthropoidea: The semicircular canal evidence. *Proc. Biol. Sci.* **279**, 3467–3475 (2012).
42. A. Le Maître, P. Schuetz, P. Vignaud, M. Brunet, New data about semicircular canal morphology and locomotion in modern hominoids. *J. Anat.* **231**, 95–109 (2017).
43. L. Rook *et al*., The bony labyrinth of *Oreopithecus bambolii*. *J. Hum. Evol.* **46**, 349–356 (2004).
44. M. S. Ponce de León *et al*., Human bony labyrinth is an indicator of population history and dispersal from Africa. *Proc. Natl. Acad. Sci. U.S.A.* **115**, 4128–4133 (2018).
45. A. Beaudet, The inner ear of the *Paranthropus* specimen DNH 22 from Drimolen, South Africa. *Am. J. Phys. Anthropol.* **170**, 439–446 (2019).
46. A. Beaudet *et al*., The bony labyrinth of StW 573 ("Little Foot"): Implications for early hominin evolution and paleobiology. *J. Hum. Evol.* **127**, 67–80 (2019).
47. J. del Rio *et al*., Allometry, function and shape diversification in the inner ear of platyrrhine primates. *J. Mammal. Evol.*, 10.1007/s10914-019-09490-9 (2020).
48. A. Urciuoli, C. Zanolli, S. Almécija, S. Moyà-Solà, D. M. Alba, Analysis of the primate vestibular apparatus: A comparison of landmark-based and deformation-based 3D geometric morphometric approaches. *Proc. Eur. Soc. Stud. Hum. Evol.* **7**, 193 (2018).
49. N. Morimoto *et al*., Variation of bony labyrinthine morphology in Mio-Plio-Pleistocene and modern anthropoids. *Am. J. Phys. Anthropol.* **173**, 276–292 (2020).
50. T. C. Rae, P. M. Johnson, W. Yano, E. Hirasaki, Semicircular canal size and locomotion in colobine monkeys: A cautionary tale. *Folia Primatol. (Basel)* **87**, 213–223 (2016).
51. M. D. Malinzak, R. F. Kay, T. E. Hullar, Locomotor head movements and semicircular canal morphology in primates. *Proc. Natl. Acad. Sci. U.S.A.* **109**, 17914–17919 (2012).
52. A. Cardini, P. D. Polly, Cross-validated between-group PCA scatterplots: A solution to spurious group separation? *Evol. Biol.* **47**, 85–95 (2020).
53. A. Perier, R. Lebrun, L. Marivaux, Different level of intraspecific variation of the bony labyrinth morphology in slow- versus fast-moving Primates. *J. Mamm. Evol.* **23**, 353–368 (2016).
54. L. A. Gonzales, M. D. Malinzak, R. F. Kay, Intraspecific variation in semicircular canal morphology—A missing element in adaptive scenarios? *Am. J. Phys. Anthropol.* **168**, 10–24 (2019).
55. Y. Kunimatsu, M. Nakatsukasa, D. Shimizu, Y. Nakano, H. Ishida, Loss of the subarcuate fossa and the phylogeny of *Nacholapithecus*. *J. Hum. Evol.* **131**, 22–27 (2019).
56. R. D. Rabbitt, E. R. Damiano, J. W. Grant, "Biomechanics of the semicircular canals and otolith organs" in *The Vestibular System*, S. M. Highstein, R. R. Fay, A. N. Popper, Eds. (Springer, 2004), pp. 153–201.
57. D. R. Begun, Phyletic diversity and locomotion in primitive European hominids. *Am. J. Phys. Anthropol.* **87**, 311–340 (1992).

58. D. R. Begun, New catarrhine phalanges from Rudabánya (Northeastern Hungary) and the problem of parallelism and convergence in hominoid postcranial morphology. *J. Hum. Evol.* **24**, 373–402 (1993).
59. S. Almécija, D. Alba, S. Moyà-Solà, M. Köhler, Orang-like manual adaptations in the fossil hominoid *Hispanopithecus laietanus*: First steps towards great ape suspensory behaviours. *Proc. Biol. Sci.* **274**, 2375–2384 (2007).
60. D. M. Alba, S. Almécija, S. Moyà-Solà, Locomotor inferences in *Pierolapithecus* and *Hispanopithecus*: Reply to Deane and Begun (2008). *J. Hum. Evol.* **59**, 143–149, discussion 150–154 (2010).
61. M. Pina, D. M. Alba, S. Almécija, J. Fortuny, S. Moyà-Solà, Brief communication: Paleobiological inferences on the locomotor repertoire of extinct hominoids based on femoral neck cortical thickness: The fossil great ape *hispanopithecus laietanus* as a test-case study. *Am. J. Phys. Anthropol.* **149**, 142–148 (2012).
62. W. Wimmer, C. Vandersteen, N. Guevara, M. Caversaccio, H. Delingette, "Robust cochlear modiolar axis detection in CT" in *Medical Image Computing and Computer Assisted Intervention–MICCAI 2019*, D. Shen *et al*., Eds. (Springer, 2019), pp. 3–10.
63. N. Jeffery, F. Spoor, Prenatal growth and development of the modern human labyrinth. *J. Anat.* **204**, 71–92 (2004).
64. L. E. Copes, W. H. Kimbel, Cranial vault thickness in primates: *Homo erectus* does not have uniquely thick vault bones. *J. Hum. Evol.* **90**, 120–134 (2016).
65. L. E. Copes, L. M. Lucas, J. O. Thostenson, H. E. Hoekstra, D. M. Boyer, A collection of non-human primate computed tomography scans housed in MorphoSource, a repository for 3D data. *Sci. Data* **3**, 160001 (2016).
66. S. Durrleman *et al*., "Topology preserving atlas construction from shape data without correspondence using sparse parameters" in *Proceedings of Medical Image Computing and Computer Aided Intervention*, N. Ayache, H. Delingette, P. Golland, K. Mori, Eds. (Springer, 2012), pp. 223–230.
67. J. Dumoncel, S. Durrleman, J. Braga, J. P. Jessel, G. Subsol, Landmark-free 3D method for comparison of fossil hominins and hominids based on endocranium and EDJ shapes. *Am. J. Phys. Anthropol.* **153**, 114 (2014).
68. A. Beaudet *et al*., Upper third molar internal structural organization and semicircular canal morphology in Plio-Pleistocene South African cercopithecoids. *J. Hum. Evol.* **95**, 104–120 (2016).
69. S. Dray, A. Dufour, The ade4 Package: Implementing the duality diagram for ecologists. *J. Stat. Softw.* **22**, 10.18637/jss.v022.i04 (2007).
70. S. Schlager, "Morpho and Rvcg—Shape analysis in R" in *Statistical Shape and Deformation Analysis*, G. Zheng, S. Li, G. Szekely, Eds. (Academic Press, 2017), pp. 217–256.
71. J. Oksanen *et al*., vegan: Community ecology package (R package version 2.5-6, 2019). https://CRAN.R-project.org/package=vegan. Accessed 12 January 2021.
72. E. Paradis, K. Schliep, Ape 5.0: An environment for modern phylogenetics and evolutionary analyses in R. *Bioinformatics* **35**, 526–528 (2019).
73. F. Savje, distances: Tools for distance metrics (R package version 0.1.8, 2019). https://CRAN.R-project.org/package=distances. Accessed 12 January 2021.
74. B. Sidlauskas, Continuous and arrested morphological diversification in sister clades of characiform fishes: A phylomorphospace approach. *Evolution* **62**, 3135–3156 (2008).
75. M. Nakatsukasa, Y. Kunimatsu, *Nacholapithecus* and its importance for understanding hominoid evolution. *Evol. Anthropol.* **18**, 103–119 (2009).
76. L. Rook, L. Bondioli, M. Köhler, S. Moyà-Solà, R. Macchiarelli, *Oreopithecus* was a bipedal ape after all: Evidence from the iliac cancellous architecture. *Proc. Natl. Acad. Sci. U.S.A.* **96**, 8795–8799 (1999).
77. B. Wood, E. K Boyle, Hominin taxic diversity: Fact or fantasy? *Am. J. Phys. Anthropol.* **159**, S37–S78 (2016).
78. D. Schluter, T. Price, A. Ø. Mooers, D. Ludwig, Likelihood of ancestor states in adaptive radiation. *Evolution* **51**, 1699–1711 (1997).
79. L. J. Revell, phytools: An R package for phylogenetic comparative biology (and other things). *Methods Ecol. Evol.* **3**, 217–223 (2012).
80. D. C. Adams, A generalized K statistic for estimating phylogenetic signal from shape and other high-dimensional multivariate data. *Syst. Biol.* **63**, 685–697 (2014).
81. D. C. Adams, M. L. Collyer, A. Kaliontzopoulou, Geomorph: Software for geometric morphometric analyses (R package version 3.1.0, 2019). https://cran.r-project.org/package=geomorph. Accessed 12 January 2021.
82. S. P. Blomberg, T. Garland Jr, A. R. Ives, Testing for phylogenetic signal in comparative data: Behavioral traits are more labile. *Evolution* **57**, 717–745 (2003).